Examining the radio to gamma-ray correlation of the blazar PKS 1424-418 during its flaring state

P. V. van Zyl and M. J. Gaylard

Hartebeesthoek Radio Astronomy Observatory, P.O. Box 443, Krugersdorp 1740, South Africa, e-mail: [pfesesani;mike]@hartrao.ac.za

Abstract. We carried out a multi-frequency cross-correlation analysis of the blazar PKS 1424-418 with data collected by Fermi Large Area Telescope (Fermi-LAT) and the Hartebeesthoek Radio Astronomy Observatory (HartRAO) 26m radio telescope between 17 October 2012 and 9 September 2013 during its flaring state. Using the discrete cross-correlation function from Edelson & Krolik (1988), we examined the data for time lags. Our results confirm the existence of a significant cross-correlation between the gamma-ray and the radio data, with the radio events being delayed relative to the gamma-ray events.

Key words. Multi-frequency observing – Blazar PKS 1424-418 – Correlation analysis

1. Introduction

Multi-frequency observations of blazar sources have become one of the few best mechanisms used to probe high energy emission regions (Urry 1996; Böttcher 2001; Patiño-Álvarez et al. 2012; Hovatta et al. 2007). Radiating large amounts of energy ($L_{agn} > 10^{40}$ erg s^{-1}), blazars exhibit extreme characteristics that include continuum emission across the electromagnetic spectrum (EM) from radio to gamma-rays, strong polarizations in both optical and radio wavelengths, and rapid variability on very short ($\sim$ hours-days, Vovk & Neronov 2013; Kraus et al. 2003) to very long ($\sim$ months-years, Villforth et al. 2009) timescales. When they have a flat emission spectrum they are referred to as Flat Spectrum Radio Quasars (FSRQ), a subclass of blazars that shows broad emission lines. Blazar sources form part of a collection of high energy emitters called Active galactic nuclei (AGN), and they also happen to be the largest identified AGN type source (Giommi & Colafrancesco 2004).

AGN can be subdivided into different types depending on the angle between the observer and the object, with each type of AGN having their own set of special characteristics that distinguish them from all the others (Urry & Padovani 1995). Blazars are the most unique of all the AGN types emitting most of their energy down a collimated radio jet within a very small angle ($\theta \simeq 1/\Gamma$, where Γ is the bulk Lorentz factor) pointed towards the observers line of sight (Blandford & Rees 1974).

At the blazar center lies a highly compact super-massive black hole (SMBH, Beckmann & Shrader 2013) fueled by the accretion of surrounding interstellar matter (ISM). This produces an energy signature that is non-thermal in nature due to the Doppler boosting of low energy photons being accelerated to higher relativistic energies. These particle in-

teractions in the radio jets produce a distinct spectral energy distribution (SED) characterized by two main bumps, one peaking in the infrared to optical frequencies due to synchrotron radiation emitted by the acceleration of particles in a magnetic field, and the other peaking in the gamma-ray frequencies (E $\gtrsim$ 1 MeV) due to Inverse Compton (IC) radiation emitted by relativistically boosted low energy photons.

Multi-wavelength high cadence observations of blazar sources provide a direct method to probe the regions nearest to the SMBH. With statistical techniques we can study the nature of the relationship between different wavelengths. Results from these studies can then be used as a means to determine the locations of the energy emitting regions and the particle content.

The work presented here sought to study the radio to gamma-ray correlation of the blazar PKS 1424-418. The main aim of this study was to examine how the low energy radio waves and high energy gamma-ray observations behaved during the multiple flaring events that occurred over the observing period. To achieve this we focused on finding answers to three main questions;

1. Did the gamma-ray flares produce an equivalent radio event?
2. What are the time-delays?
3. Is there any periodicity associated with the gamma-ray events?

2. PKS1424-418

PKS 1424-418 (J1427-4206) is an FSRQ blazar located at a redshift of z=1.522. It recently underwent a series of flaring events rising from an average daily gamma-ray flux of about 0.6-1.2 $\pm$ 0.2 x 10^{-6}ph cm^{-2} s^{-1} (Ojha & Dutka 2012) to a maximum of about 2.3 $\pm$ 0.4 x 10^{-6}ph cm^{-2} s^{-1} over the observing period. In January 2013 alone the radio flux density observed using the HartRAO 26m dish at 8.4 GHz had risen from about 6.1 Jy to 7.0 Jy with 1σ uncertainties of $\pm$ 0.05 Jy (Nemanashi, Gaylard & Ojha 2013). This source increased in brightness at a remarkably fast rate since the initial gamma-ray flare event in both the gamma-rays and the radio waves.

3. Observations and data collection

This work is based on quasi-simultaneous observations of the source PKS 1424-418 conducted with the Fermi-LAT and HartRAO 26m telescopes.

3.1. Gamma-ray observations

The Fermi-LAT located on the Fermi Gamma-ray Space telescope (Fermi-GST) is a wide field of view (FOV > 2.4 sr at 1 GeV) telescope with an 8000 cm^2 effective area, designed to detect high energy gamma-rays (E > 20 MeV to over E $\sim$ 300 GeV, Atwood et al. 2009). Each time Fermi does observations the Fermi Flare Advocate (Ciprini & Thompson 2013) Gamma-ray Sky Watcher (FA-GSW) [1] releases a brief weekly memo on the high energy activity of a selection of blazars. If the blazars release energy E > 10^{-6}ph cm^{-2} s^{-1}, an ATel (Astronomers Telegram)[2] is sent out to the astronomical community notifying them of the flaring event.

The source PKS 1424-418 began flaring in October 2012, and an ATel was sent out on the blazar's activity (ATel #4494) by Ojha & Dutka 2012. This bright low-frequency peaking (ν_{peak} < 10^{14} Hz) blazar had achieved a gamma-ray peak flux of 1.4 x 10^{-6}ph cm^{-2} s^{-1}. This ATel triggered quasi-simultaneous follow up observations to monitor the radio emission of the source with the HartRAO 26m radio telescope (see § 3.2). The source flared again in January 2013 (ATel #4714 D'Ammando et al. 2013) peaking at 2.3 x 10^{-6} ph cm^{-2} s^{-1} which was brighter than all previous flares since Fermi began observations of this source. Table 1 lists all known ATels sent out to date together with the corresponding energy fluxes.

All Fermi-LAT data used in this study was obtained pre-processed in standard flux density units (Ojha, private correspondence) for data collected in the energy range E > 100 MeV, between 17 October 2012 and 9 September 2013.

---

[1] http://fermisky.blogspot.com
[2] http://www.atel.com

Table 1. PKS 1424-418 ATel sightings obtained from the ASI Science Data Center (ASDC) website http://www.asdc.asi.it/feratel/. Flux ATel is the maximum flux density reached by PKS1424-418 during the observing periods stated in the corresponding ATel's.

Date of flare	Flux (x10^{-8}) (ph cm^{-2}s^{-1})	Fermi-LAT ATel#	Radio ATel#
30/06/09	60	2104	-
21/04/10	100	2583	-
05/05/11	110	3329	-
15/10/12	140	4494	-
06/01/13	230	4714	4819

3.2. Radio observations

We began radio monitoring observations of the source PKS 1424-418 in October 2013 using the HartRAO 26m telescope in South Africa. The source is continuously observed on daily intervals at four central frequencies, 2.3 GHz (HPBW $\sim$ 21') and 12.2 GHz (HPBW $\sim$ 4') using single beam uncooled receivers, and 4.8 GHz (HPBW $\sim$ 10') and 8.4 GHz (HPBW $\sim$ 6') using dual beam Dickie switched cryogenically cooled receivers.

Radio observations are done using the drift scan technique, which is when the telescope is parked a little west of the current position of the radio source in the sky, and we use the rotation of the Earth to take continuous flux density measurements of the source. As the source passes over the fixed radio dish it produces a beam pattern output as shown in Fig. 1. Pointing errors due to atmospheric effects can occur during observations, therefore scans pointed at the half-power North (HPN) and the half-power South (HPS) points of the source are also taken to apply corrections to the peak intensity.

We obtain on average two scans per day per frequency band in both left and right circular polarization (LCP, RCP) with the exception of days when the telescope is used for VLBI observing.

4. Data reduction

4.1. Data calibration

The data was calibrated against a well known flux calibrator source, Hydra A (3C218). Hydra A is a bright radio source that shows very little or no variability in flux density over time. The calibrator source was observed at the same frequencies as the target source and using the same drift scan method.
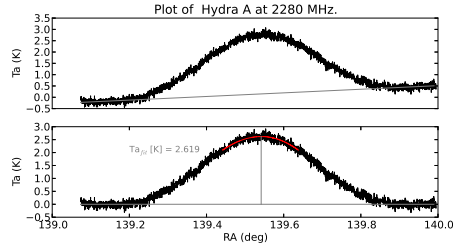
Fig. 1. The figure shows a drift scan plot of the calibrator source Hydra A. The top figure shows the drift scan from the raw data before reductions. The bottom figure shows the same drift scan after data reduction. The red line shows an estimate parabolic peak fit to the top 20% of the data. Ta$_{fit}$ is the maximum antenna temperature for the fit in Kelvins.

4.2. Quality checks for outlier detections

The raw data from the drift scans were plotted for each of the frequencies observed and then visually inspected for any irregularities. Data containing RFI (Radio Frequency Interference), step changes possibly due to receiver instabilities and bumps in the data due to poor weather conditions were considered outliers and removed, thus improving the quality of the data to be used for further analysis. Changes in the average system temperature were also used as an outlier detector, following the 2.7σ error cutoff.

4.3. Data fitting

First order baselines were subtracted from the data to remove any instabilities in the drift scan that may have been caused by the changes in

the telescope's surroundings. To find the peak antenna temperature, second order polynomials were fitted to the top 20% of the scans. As an example, Fig. 1 shows a typical beam pattern of a drift scan of Hydra A at 2.3 GHz both before and after the data was reduced and calibrated. Due to the narrower beam widths at higher radio frequencies (4.8, 8.4 and 12.2 GHz) we also had to correct for additional pointing errors in the on-source scans.

4.4. Flux density calculations

Following work done by Ott et al. (1994) we calculated the flux density of the target source using the known flux density of the calibrator Hydra A. We then used the calibrator point source sensitivity (PSS) as an antenna temperature conversion measure to determine the total flux density of PKS 1424-418. The flux density estimates for each observing day were used to create the light-curves shown in Fig. 2. The errors in the flux density of the source were assumed to be due to the scatter in the data. Only errors that fell within 2.7σ were used in the final data output. We opted to use 2.7σ errors rather than 3σ errors because they reduced the outlier contamination better than the latter.

5. Data analysis

5.1. Correlation analysis

Studying the relationship between the emission from two different wavelengths is one of the most common ways used to probe AGN as multi-wavelength observing is not always possible. The correlation between two light-curves can help understand the physical processes between certain regions of the AGN. We examined the correlation between the light-curves from the gamma-rays and radio waves using the Discrete correlation function (DCF) by Edelson & Krolik (1988). Given two light-curves a and b, the DCF calculates the cross-correlation function of the light-curves using

$$DCF_{ij} = \frac{1}{N}\left[\sum \frac{(a_i(t) - \bar{a})(b_j(t) - \bar{b})]}{\sqrt{(\sigma_a^2 - e_a^2)(\sigma_b^2 - e_b^2)}}\right] \quad (1)$$

where $\bar{a}$ and $\bar{b}$ are the means, σ_a and σ_b the standard deviations, and e_a and e_b are the errors of the respective light-curves. The DCF estimates an unbinned cross-correlation function for all measured pair points (a_i,b_j), then averages it over a pairwise lag $\Delta t_{ij} = t_j - t_i$ within the range $\tau - \Delta\tau/2 < \Delta\tau < \tau + \Delta\tau/2$ where τ is the time-lag and $\Delta\tau$ is the chosen bin width and N is the number of the unbinned entries. We estimated the errors in the time-lags as the scatter in the unbinned entries of the DCF terms. Designed to work with unevenly sampled light-curves, the DCF makes no prior assumptions about the data and only calculates the correlation and time-lags for the data sample without the interpolation of missing data.

5.2. Periodicity

The measured gamma-ray flux showed rapid variations over time that appeared to be almost periodic in nature (Fig. 2). To investigate this trend we conducted a periodogram analysis using the period detection method from Lomb (1976) that is designed for period searches in unevenly sampled data. The significance of the detection was then analyzed using the false alarm probability method from Scargle (1982). Periods have been found to exist within gamma-ray data (Nishikawa 1999), but the topic of gamma-ray periodicity has been poorly studied and the short nature of the flaring events make it almost impossible to conclude definitively on the results as a minimum of four cycles is required and hard to achieve with most rapid flares.

6. Results

Results presented here are from the sample of data collected between 17 October 2012 and 09 September 2013. From our analysis we aimed at answering three main question;

1. Did the gamma-ray flares produce an equivalent radio event?
The radio light-curves from our sample show a sharp increase after the first recorded gamma-ray flare event (MJD 56215, Nemanashi, Gaylard & Ojha 2013) for all observed

frequencies. The gamma-rays show the fastest variability with flaring events lasting only a few months, while the equivalent radio events show variability on the order of a year with higher radio frequencies showing a turnover in flux on shorter time scales (see Fig. 2).
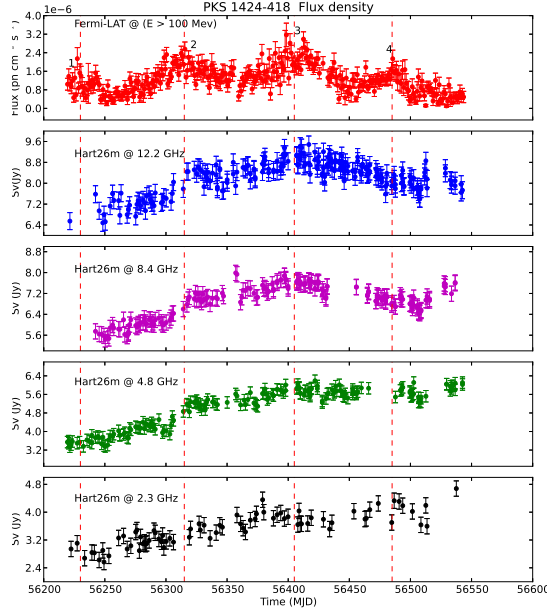
Fig. 2. Gamma-ray and radio light-curves for the source PKS 1424-418. The top section shows the light-curve from data collected by the Fermi-LAT for E > 100 MeV. Flaring events are marked by numbers 1 to 4. The second third, fourth and fifth sections show the radio light-curves from data collected by the HartRAO 26m telescope at frequencies of 12.2, 8.4, 4.8 and 2.3 GHz respectively.

2. What are the time-delays?

From the DCF results, the gamma-ray and radio data seem to correlate well, with the gamma-rays leading the radio data. Results of the correlation analysis are listed in Table 2 and are consistent with the literature (e.g. Ghirlanda et al. 2010) where the time delay decreases with increasing frequency. During flaring the higher energy particles escape easier than their lower counterparts which is consistent with what we see in our results.

Correlations conducted on the radio to radio relationships also showed a higher frequency lead compared to the lower frequencies. However, the correlation between the 12.2 and 8.4 GHz frequencies showed the reverse with a time delay of $\tau_{12.2-8.4GHz}$ = -4.9 ± 0.6 days.

All correlation results were estimated with different bin widths of the DCF based on the number of data points available at the different frequencies to produce a smooth enough correlation for a peak fitting algorithm to determine the lag times. This selection may bias the outcome of the results and require some caution when selecting DCF parameters.

Table 2. Time delay results from the correlation analysis.

Gamma (γ) / radio correlation	Time delay (τ)
$\tau_{\gamma-12.2GHz}$	23.2 ± 1.1 days,
$\tau_{\gamma-8.4GHz}$	27.9 ± 1.8 days
$\tau_{\gamma-4.8GHz}$	68.8 ± 1.4 days
$\tau_{\gamma-2.3GHz}$	70.2 ± 2.4days
Radio / radio correlation	Time delay (τ)
$\tau_{12.2-8.4GHz}$	-4.9 ± 0.6 days
$\tau_{12.2-4.8GHz}$	4.8 ± 1.1 days
$\tau_{12.2-2.3GHz}$	13.8 ± 3.1 days
$\tau_{8.4-4.8GHz}$	3.9 ± 1.7 days
$\tau_{8.4-2.3GHz}$	10.4 ± 2.3 days
$\tau_{4.8-2.3GHz}$	4.7 ± 2.9 days

3. Is there any periodicity associated with the gamma-ray events?

The results from the Lomb period detection method show both a long term and a short term gamma-ray power spectrum variation indicated by the black and blue lines respectively in the frequency domain (Fig. 3). After converting the frequency related to the peak power into the period domain, we obtain an 86.2 day period for the short term variation. This result correlates well with the gamma-ray short term flare variation shown in Fig. 2. The period detected appeared to be significant following the Scargle false alarm method. This is shown by the peak appearing above the significance line shown in red which lies well beyond the zero noise level.
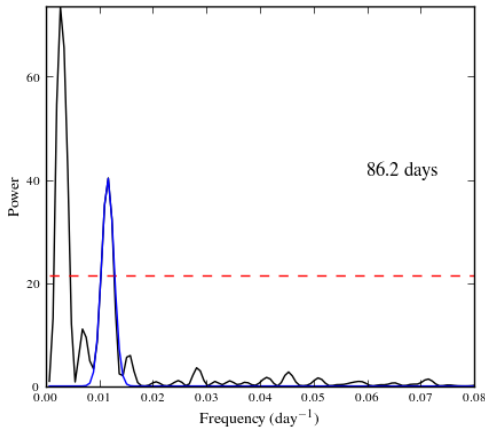
Fig. 3. The figure shows a periodogram of the gamma-ray data in the frequency domain for the source PKS 1424-418. The blue line shows the short term power spectrum variation and the black line shows the long term power spectrum variation.

7. Conclusion & future work

Although the results presented here are from a limited data set, the analysis show a definite connection between the gamma-ray and radio data. Whether we can connect each gamma-ray flare to individual radio flares is a question that can only be answered by getting more data. We will continue to monitor PKS 1424-418 to assess the long term variability of the source with high cadence observations. We will also perform an O-C (Observed vs Calculated) analysis to determine whether the periodicity found in the gamma-ray data is real. VLBI (Very Long Baseline Interferometry) radio observations of PKS 1424-418 show both flux and structural variability of the source on milliarcsecond scales. For future work, we plan to investigate any connection between the structural variability of the source seen on VLBI scales and the flaring events evident in the single dish monitoring data.

References

Atwood, W. B. et al. 2009, ApJ, 697, 1071

Beckmann, V. & Shrader, C. R. 2013, in Proc. of "An INTEGRAL view of the high-energy sky (the first 10 years)" - 9th INTEGRAL Workshop and celebration of the 10th anniversary of the launch (INTEGRAL 2012), Bibliotheque Nationale de France, 15-19 October 2012, Paris, France., 69

Blandford, R. D. & Reese, M. J. 1974, MNRAS, 169, 395

Böttcher M. 2001, Bulletin of the Astronomical Society of India, 30, 115

Ciprini, S. & Thompson, D. J. 2013, arXiv:1303.4054v1

Collmar, W. et al. 2000, A&A, 354, 513

D'Ammando, F., et al. 2014, ATel, 4714

Edelson, R. A. & Krolik, J. H. 1988, ApJ, 333, 646

Giommi, P. & Colafrancesco, S. 2004, A&A, 414, 7

Ghirlanda, G. et al. 2010, MNRAS, 413, 852

Hovatta, T., et al. 2007, A&A, 469,899

Kraus, A., et al. 2003, A&A, 401, 161

Lomb, N. R. 1976, Ap&SS, 39, 447

Nemanashi, P., Gaylard, M. J., & Ojha, R. 2013, ATel, 4819

Nishikawa, D. 1999, arXiv:astro-ph/9906087v1

Ojha, R. & Dutka, M. 2013, ATel, 4494

Ott, M., et al. 1994, A&A, 284, 331

Patiño-Álvarez, V., et al. 2012, arXiv:1303.1898v1

Scargle, J. D. 1982, ApJ, 263, 835

Urry, C. M. & Padovani, P. 1995, PASP, 107, 803

Urry, C. M. 1996, in Proc. of Astronomical Society of the Pacific Conf. Ser., 110, 391

Villforth, C. et al. 2009, MNRAS, 402, 2087

Vovk, I. E. & Neronov, A. 2013, ApJ, 767, 103